



TSF0009

## Heat transfer enhancement underneath inline merging turbulent spots

Sudarat Srichan, Jirachai Mingbunjerdasuk, and Weerachai Chaiworapuek\*

Department of Mechanical Engineering, Faculty of Engineering, Kasetsart University,  
50 Ngamwongwan Road, Ladyao, Chatuchak, Bangkok 10900, Thailand

\* Corresponding Author: fengwcc@ku.ac.th, Telephone Number: 0-2797-0999#1868,  
Fax Number: 0-2579-4576

**Abstract.** A turbulent spot is a small turbulent patch and surrounded by laminar flow. In this paper, its behavior after merging longitudinally with the neighbours is investigated using thermochromic liquid crystals during the local Reynolds number between 61,000 and 130,000. Each turbulent spot is generated artificially via a 1 mm diameter hole with an interval of 1 s apart. From the flow visualization technique using the liquid crystals and the image processing method, the thermal characteristics of turbulent spot was obtained as the contours of Nusselt number and the turbulent spot effectiveness. The average Nusselt number and effectiveness inside the spot footprint are time-dependently reported. The results of heat transfer enhancement of the single spot and two spots are compared and discussed. These obtained results will be important information in order to develop the process of heat transfer augmentation over the flat plate flow.

### 1. Introduction

Nowadays, heat transfer techniques are commonly used in various engineering areas such as air-conditioning equipment, evaporators, process industries, thermal power plants, refrigeration systems, etc. in order to decrease cost by increase the system efficiency. Three different techniques of heat transfer enhancement, including passive, active and compound techniques are then used gain the thermal efficiency, leading to the higher overall efficiency. The passive technique doesn't need any external power input, e.g. rough surfaces, extended surfaces, displaced enhancement devices, swirl flow devices and additives for liquids or gases. On the other hand, the active technique involves some external power input for the enhancement of heat transfer such as mechanical aids, surface vibration, fluid vibration, injection, jet impingement, etc. Meanwhile, the compound technique involves complex design and hence has limited applications. Nevertheless, it has been found that a turbulent spot, which can be artificially initiated on the flat plate under the laminar boundary layer has a potential to augment the heat transfer. With a small input power for the spot generation, the turbulent spot can gain the heat transfer rate up to 15 % during  $Re_x = 60,000 - 130,000$  [1]. Furthermore, this heat rate is still increasing when the turbulent spot propagates further downstream.

Thus, this research investigates the thermal behavior of the heating flat plate underneath the turbulent spots, artificially initiated by 2 pulsating water jets with the duration of 1 s apart. The jets are injected in upward direction, perpendicular to the mainstream flow to disturb the laminar boundary layer and cause the inline (tandem) merging process of the spots. In this paper, the flow visualization

technique using thermochromic liquid crystals (TLCs) are well explained and used to measure the unsteady surface temperature. With the aid of image processing technique and energy balance, the time-dependent Nusselt number and turbulent spot effectiveness are determined. Also, the thermal characteristics between the tandem merging spots and the single turbulent spot are compared and discussed.

## 2. Literature review

### 2.1. Single turbulent spot and merging turbulent spots

Following the chaotic level, the fluid flow can be classified using Reynolds number ( $Re$ ) as laminar, transition, and turbulent flows. When the  $Re$  is more than the critical Reynolds number, the flow is considered as turbulent flow, otherwise it is laminar. The turbulent spot is important phenomena under boundary layer transition and found as a small turbulent patch, surrounding by laminar flow. Emmons [2] who first discovered the turbulent spot and suggested that the distribution of intermittency factor in the transition region could be described as a function of the parameters such as growth rate, convection velocity and spot production rate. His model treated the turbulent region in a transitional boundary layer as the simple superposition of independently developed turbulent spots. Afterwards, Elder [3] and Sokolov et al. [4] verified that two partially merging turbulent spots occupied almost the same turbulent area as the simple superposition of their outlines. From Emmons's assumption, showing that no interaction between spot, Shubauer and Klebanoff [5] investigated the spot behavior experimentally using hotwire anemometer and they also described the spot features such as leading edge, trailing edge, becalmed region, etc. as figure 1. The shape of turbulent spot exhibited an arrowhead-like structure. The velocity of leading edge and trailing edge are 88 % and 50 % of freestream velocity, respectively. In 1976, Wygnanski [6] postulated that a spot grows in the streamwise direction by the continual addition of hairpin vortices at the spot trailing edge. With the advection and merging processes of the turbulent spots, these isolated hairpin forests develop into the downstream turbulent region [7]. Hence, the increase of heat transfer rate, occurring in the transition region is mainly caused by the turbulent spots. Particularly, the highest surface heat transfer occurs at the trailing or calmed region of a turbulent spot, regardless of maturity [1].

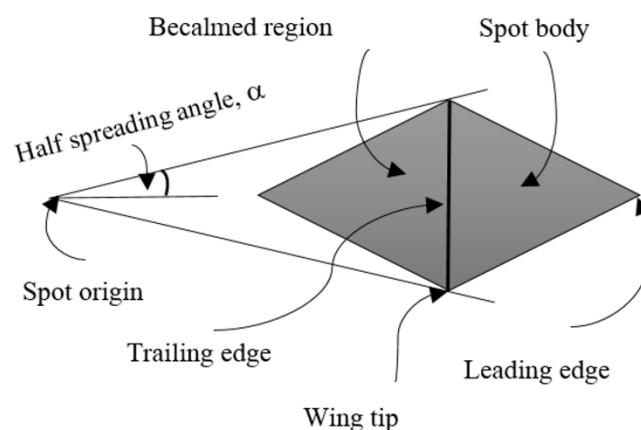


**Figure 1.** Schematic drawing of a turbulent spot.

Makita and Nishizawa [8] studied a merging process of a pair of turbulent spots using the multi-hotwire system. They discovered that when two turbulent spots merge with each other, interaction between the longitudinal wing tip vortices gives birth to a strong upwash in the merged region. This strong upwash induces an inflectional velocity profile and then enhances spanwise vortices at the top of the merged spot. Krishnan and Sandham [9] used Direct Numerical Simulation (DNS) to verify mechanism of inline merging and discovered that calmed region behind the tail of the downstream spot is found to suppress the growth of the upstream spot. The upstream spot is ultimately engulfed by

the downstream spot and by a longitudinal merging effect may be responsible, rather than a decay in the perturbation energy [10].

## *2.2. Thermochromic liquid crystal*

In 1888, Reinitzer [11] carried out the experiment on the cholesteryl benzoate and first discovered the birefringence properties of liquid crystals. Thermochromic liquid crystals - TLCs have been widely used by researchers in heat transfer and fluid flow communities as a thermal imaging tool to show surface and spatial temperature distributions. They are essentially characterized by a helical molecular structure, stretching as a function of temperature. When illuminated with white light, the liquid crystals selectively reflect monochromatic light with a wavelength that equals to the pitch of the helical structure. When their temperature is increasing, the wavelength of the reflecting light changes from red to blue through the visible spectrum. Calibration process is first necessary to define the color-temperature relationship of the liquid crystals in order to apply them for the quantitative temperature measurements. Abdullah et al. [12] provided useful information to novice and intermediate users for the calibration process of the liquid crystals, particularly for surface thermography. Furthermore, Wiberg and Lior [13] reported that the important error, affecting the precision of liquid crystals includes hysteresis, aging, surrounding illumination disturbance, viewing angle, amount of light into the camera, and coating thickness.

## **3. Experimental Method**

### *3.1. Experimental setup*

This experiment was conducted in a rectangular water flow channel which had a 0.15 m width, a 0.2 m height and a 1 m long as shown in figure 2. It was made from acrylic of 1 cm thick in order to obtain a good view and provide the resistance for the heat loss. The bleeding channel was installed at the inlet of test plate to bleed the water out and refresh a new boundary layer on the test surface made by an aluminum plate. This surface was covered by a black polyvinyl chloride (PVC) sheet of 0.12 mm thick. The thermochromic liquid crystals (TLCs) were coated on the PVC sheet to measure the temperature distribution of the test plate. They are over coated by a layer of varnish in order to prevent the direct contact between the TLCs and water flow, which can deteriorate the birefringence properties of liquid crystals. In this study, the active range of TLCs is from 26 °C to 30 °C so the experiment was conducted during this temperature range. Three type-K thin leaf thermocouples, having an uncertainty of 0.75 % are well glued on top of the test plate at the streamwise position of 0.364, 0.469 and 0.626 m from the plate leading edge. The temperature, measured by these thermocouples was directly send the data logger and correlated with the color of the liquid crystals.

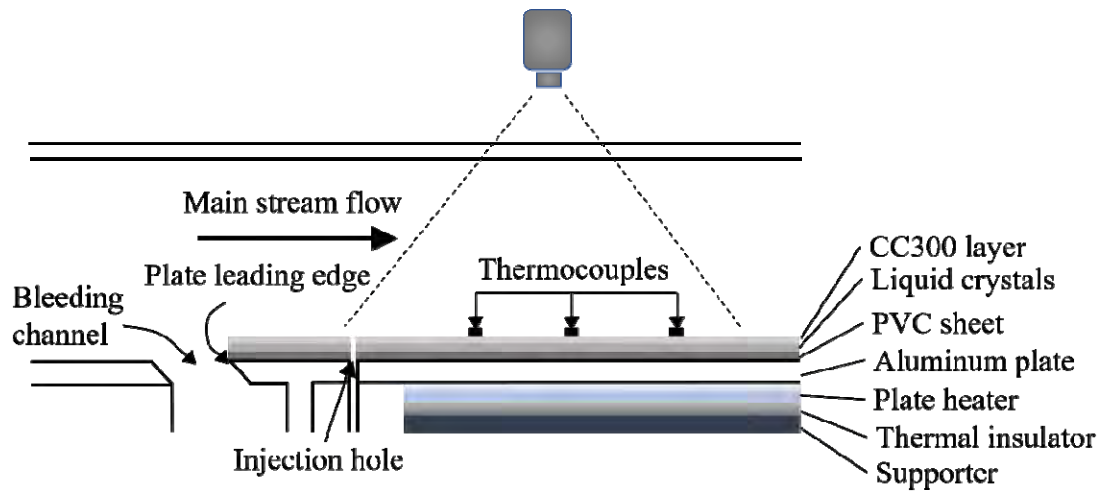


**Figure 2.** Schematic diagram of the test section in the water tunnel.

In order to perform an isothermal surface, six commercially plate heaters with the different size were installed under the aluminum plate. They were also controlled by using a proportional integral derivative controllers (PID) and dimmers. Hence, the constant temperature surface condition can be obtained at 24 °C through the experiment. In the meantime, the mainstream flow at 0.17 m/s was supplied by a 2.5 HP centrifugal pump. This velocity corresponds to the local Reynolds number of the test region during 61,000 – 130,000. The turbulent spot was created by injecting the water through a 1 mm diameter hole in perpendicular direction of the main stream flow to disturb the boundary layer at 0.3 m from the plate leading edge. At this position, the boundary layer profile and thickness was measured using a hot film sensor as depicted in figure 3. The results show that the yielded data agree well the Blasius profile and the laminar boundary layer thickness is  $\delta_0 = 0.006$  m, referring to the boundary layer displacement thickness,  $\delta^*$  of 0.002 m. The turbulence intensity of the freestream flow is 1.12 %.

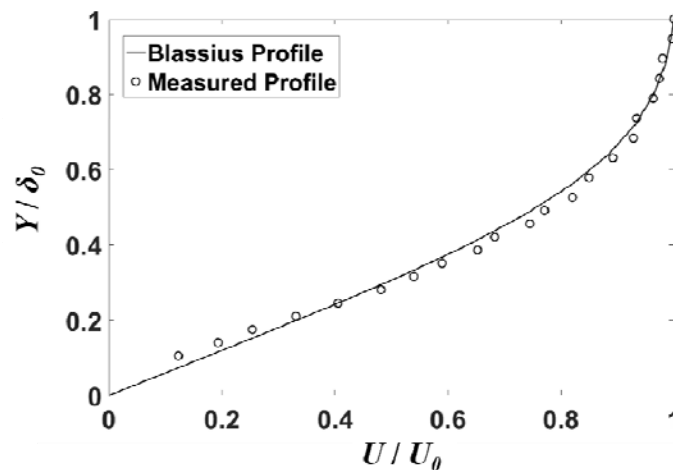


**Figure 3.** Measured boundary layer profile at the location of spot generator, where  $U$  is the measured velocity (m/s);  $U_0$  is the free stream velocity (m/s);  $y$  is the height of measuring position (m);  $\delta_0$  is the laminar boundary layer thickness (m).

The injector is directly connected with the pressure system as shown in figure 4. The water in this system was fed from the water tank and its pressure was controlled by a diaphragm tank, mounted with the air pump to keep the pressure at 3 bars through the test. Afterwards, each trigger was done

manually with help of the programmable logic controller (PLC) system via a solenoid valve. Thus, the injection was kept at the period and velocity of 0.1 s and 13 m/s, respectively.

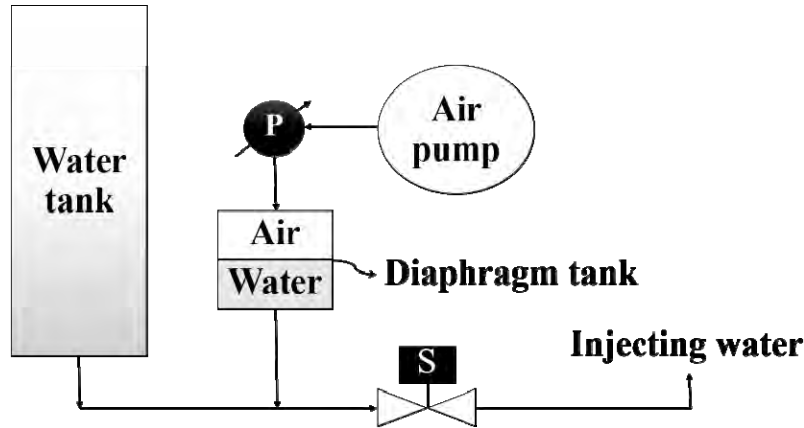


**Figure 4.** Pressure system of the spot generator.

Two fluorescent bulbs having diameter of 2.5 cm was installed beside the test section to illuminate the white light on the coating TLCs. Their light intensity was strengthened by a glossy reflector, mounted with each bulb. A video camera was installed at 1.5 m above test surface to record the color change of liquid crystals with the frame rate of 25 fps.

### 3.2. Mathematical analysis

Before use, the color of thermochromic liquid crystals must be correlated via a calibration process with method following Chaiworapuek and Kittichaikarn [14]. In the experiment, the video camera firstly collected the images in RGB system, comprising Red, Green, and Blue signals. For the convenience of the calculation, this system was changed to HSI system or Hue, Intensity, and Saturation signals. The relation between Hue and RGB system is given by Russ [15] as:

$$H = \cos^{-1}(Z) \quad \text{if} \quad G \geq R \quad (1)$$

$$H = 2\pi - \cos^{-1}(Z) \quad \text{if} \quad G < R \quad (2)$$

$$Z = (2B - G - R) / (2 * [(B - G)^2 + (B - R)(G - R)]^{1/2}) \quad (3)$$

Where  $H$  = Hue signal value  
 $R$  = Red signal value  
 $G$  = Green signal value  
 $B$  = Blue signal value

The relation between Hue and surface temperature in calibration process must be obtained at the same condition as the turbulent spot test. Each color of liquid crystals at a thermocouple is recorded through the temperature from 25.8 °C to 28.2 °C with an increment of 0.2 °C. The relation between color of liquid crystals and surface temperature was fit by 3<sup>rd</sup> order polynomial equation as shown in figure 5. This equation has the  $R^2$  of 0.9803 and is given as:

$$T = 91.11H^3 - 111.25H^2 + 48.887H + 18.424 \quad (4)$$

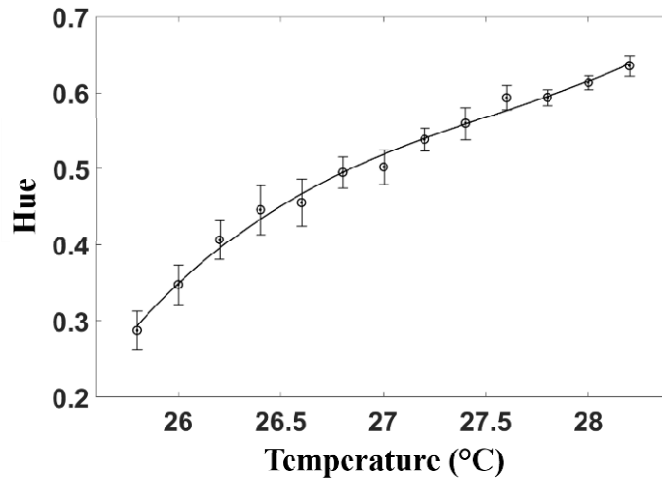


**Figure 5.** Calibrated relation between hue and temperature.

The local Reynolds number on the flat plate can be determined as:

$$Re_x = \rho U_0 x / \mu \quad (5)$$

Where  $\rho$  = density of water (kg/m<sup>3</sup>)  
 $U_0$  = freestream velocity (m/s)  
 $x$  = streamwise distance from the plate leading edge (m)  
 $\mu$  = dynamic viscosity of water (kg/m·s)

Following Kays et al. [16] the local Nusselt numbers for laminar flow and heat transfer coefficient can be determined as:

$$Nu_x = [0.332 Re_x^{1/2} Pr^{1/3}] / [1 - (\zeta / x)^{3/4}]^{1/3} \quad (6)$$

Where  $Pr$  = Prandtl number  
 $\zeta$  = unheated starting length (m)

The obtained heat flux is explained from Newton's law of cooling, so can be determined as:

$$q_x = h_x(T_s - T_0) \quad (7)$$

and Nusselt numbers determined as

$$Nu_x = h_x x / k \quad (8)$$

Where  $q_x$  = heat flux (W/m<sup>2</sup>)  
 $h_x$  = local heat transfer coefficient (W/m<sup>2</sup>·°C)  
 $T_s$  = surface temperature (°C)  
 $T_0$  = freestream temperature (°C)  
 $k$  = thermal conductivity (W/m·°C)

The local Nusselt number on the heating surface without the turbulent spot obtained in this study was validated with those from the correlation of Kays et al. [16] as depicted in figure 6. The comparison shows that they are consistent during the local Reynolds number between 61,000 and 130,000. This confirm the reliability of the experimental set up of the current study.

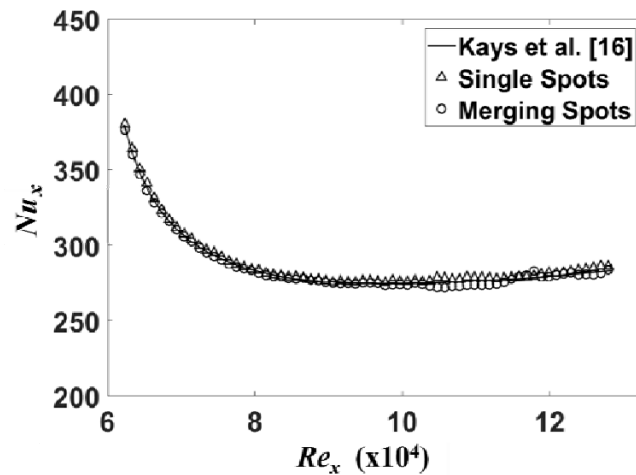


**Figure 6.** Comparison of the local Nusselt number from the experiment and the results calculated by correlation of Kays et al. [16].

The dimensionless of time  $\tau$  is used to define the floating time after the spot initiation. It can be determined as:

$$\tau = t / (\delta^* / U_0) \quad (9)$$

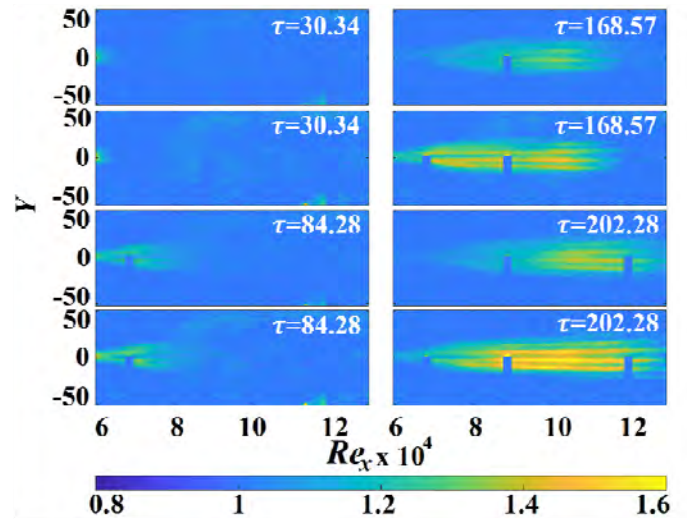
Where  $t$  = time (s)

$\delta^*$  = boundary layer displacement thickness at the water injection (m)

In the present experiment, the second turbulent spot was generated after the first spot 1 second, corresponding to the  $\Delta\tau$  of 84.16.

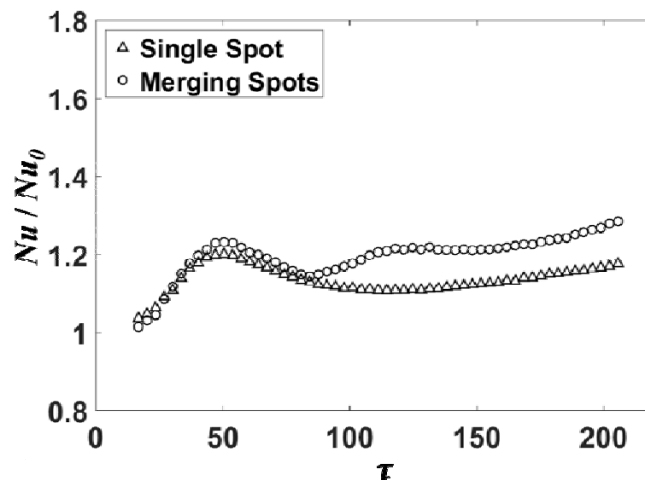
#### 4. Results and Discussions

In this study, the images of the test region were recorded in RGB format. They were changed to Hue signal and the surface temperature via Equation 1 – 3 and Equation 4, respectively. Fig. 7 presents the contour of  $Nu / Nu_0$  of single spot and merging spots at  $\tau$  between 30.34 and 202.28 where  $Nu$  and  $Nu_0$  is the local Nusselt number of the heating surface under the condition with and without turbulent spot, respectively. The magnitude is between 0.8 – 1.6, presented in the below color bar. The x axis refers the  $Re_x$  during 61,000 – 130,000 while the dimensionless spanwise distance, equaling  $Y = y / \delta^*$  are between -50 and 50. In the figure, three blue vertical strips are the location of the thin leaf thermocouples. At each  $\tau$ , the upper and the lower windows depict the  $Nu / Nu_0$  of the single turbulent spot and merging turbulent spots, respectively. The figure shows that the turbulent spots are initiated by the water injection and have the streaky structure as those yielded by Rakpakdee and Chaiworapuek [17]. They enhance the heat transfer of the heating surface and the maximum Nusselt number appears at the center of the spot. This are increasing when it convects further downstream.



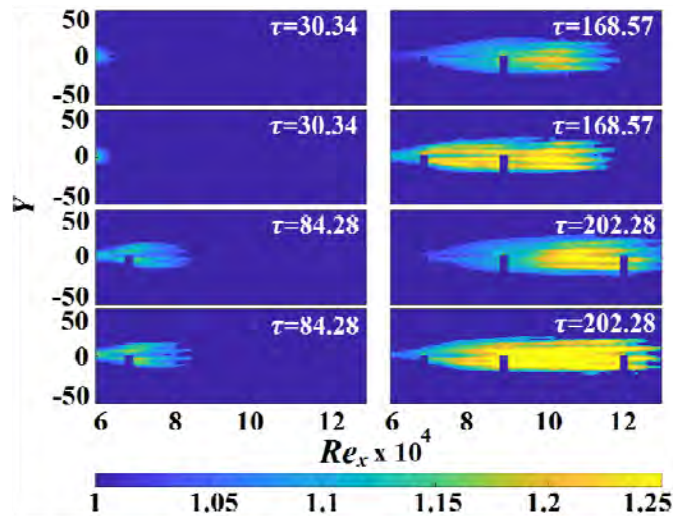
**Figure 7.** The contour of  $Nu / Nu_0$  of single spot and merging spots at  $\tau = 30.34, 84.28, 168.57,$  and  $202.28$ .

At  $\tau = 202.28$ , the maximum magnitude of  $Nu$  occurs at the core of the structure. It is 40 % increase above those under the laminar boundary layer. When the single spot is compared with the lower window, they behave similarly at  $\tau = 30.34$  because the second spot haven't been initiated yet. At  $\tau = 84.28$ , the second pulse has been already injected to create the second turbulent spot since  $\tau = 84.16$ . This creation results in the higher  $Nu / Nu_0$  at the upstream region comparing with the single spot at  $\tau = 168.57$ . At this point, the maximum magnitude is approximately 40 % above the laminar state. It is up to 60 % when the spots fully unites at  $\tau = 202.28$ . The average  $Nu / Nu_0$  inside the turbulent spot bound is plotted against the  $\tau$  as shown in figure 8. The results of single spot are in agreement with those yielded from Chaiworapuek and Kittichaikarn [14]. The first maximum of 1.2 is from the effect of the water injection while the second increase appears after  $\tau$  of 120 due to its maturity. Meanwhile, the characteristic of Nusselt number ratio is consistent with the result of single spot. After the second pulse is injected at  $\tau = 84.16$ , the magnitude of  $Nu / Nu_0$  increases again and it is relatively higher than those obtained from single turbulent spot. At  $\tau > 210$ , the average  $Nu / Nu_0$  through the spot structure is more than 40 % above the laminar level.



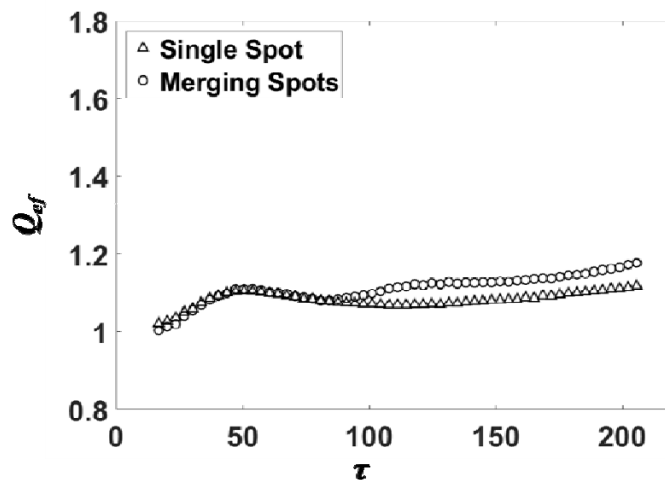
**Figure 8.** The comparison of  $Nu / Nu_0$  between single spot and merging spots.

The contours of the turbulent spot effectiveness,  $Q_{ef} = q_s / q_{ns}$  are presented at  $\tau = 30.34, 84.28, 168.57,$  and  $202.28$  as depicted in figure 9. The  $q_s$  and  $q_{ns}$  are the heat flux in the spot bound under the condition with and without turbulent spot, respectively. Its magnitude of  $1 - 1.25$  can be evaluated from the below color bar. Typically, the heat transfer area in  $Q_{ef}$  contours can represent the spot structure [14]. The characteristic of the  $Q_{ef}$  is similar as the ration of Nusselt number. However, percent increase above the laminar level is different with the  $Nu / Nu_0$  distribution. The maximum  $Q_{ef}$  of the merging spot is more than 1.25 and also more than the value achieved from a single spot. Moreover, the size of merging spots is apparently bigger than the single spot, especially in streamwise direction.



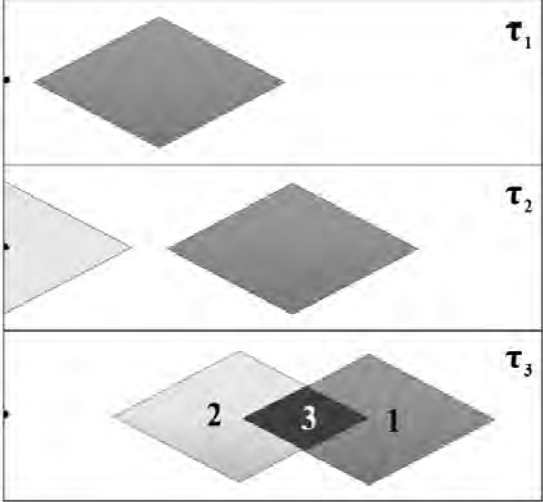
**Figure 9.** The contour of  $Q_{ef}$  of single spot and merging spots at  $\tau = 30.34, 84.28, 168.57,$  and  $202.28$ .

Figure 10 illustrates the characteristic of the average  $Q_{ef}$ , determined inside the spot bound during  $\tau = 0 - 210$ . For both cases, the maximum  $Q_{ef}$  at the early state is about 1.11. After the  $Q_{ef}$  of single spot reaches the minimum value after the first peak, the magnitude increases again by the effect of the spot maturity. Also, the comparison of  $Q_{ef}$  of single spot and merging spots against  $\tau$  clearly shows that the merging spots provide more  $Q_{ef}$  than those yielded from single spot since  $\tau = 84.28$ . However, the similar tendency between them can be seen.



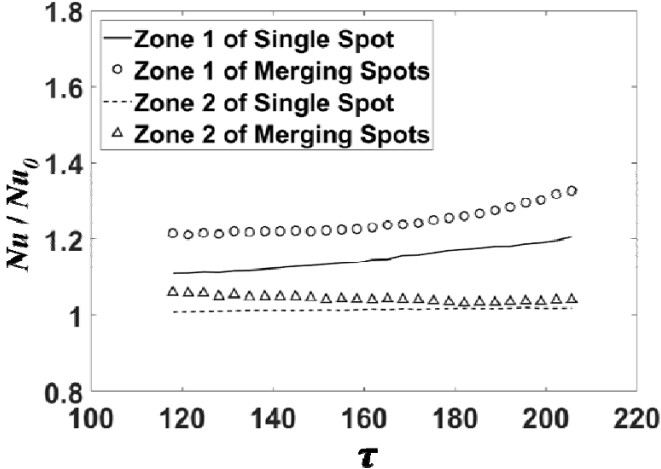
**Figure 10.** The comparison of  $Q_{ef}$  between single spot and merging spots

In order to study the thermal behavior of the spots after merging process, the consideration must be taken place separately as leading and following spots. The intersecting and non-intersecting regions are presented as depicted in figure 11. The first window in the figure shows the turbulent spot, propagating downstream from left to right at  $\tau_1$ . When the second spot appears at  $\tau_2$  and combines with the first turbulent spot at  $\tau_3$ , the zone 1, 2 and 3 are defined as the non-intersecting region of the leading and following spot and the intersecting region. Thus, these zones will be later used to describe the region inside the merging spots.



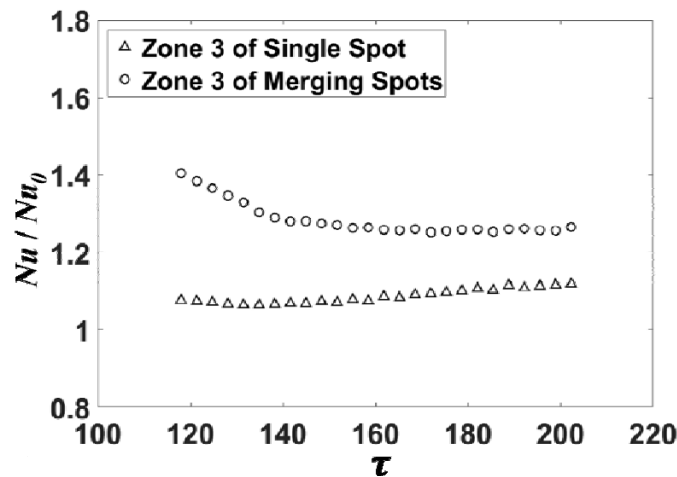
**Figure 11.** Inline merging process.

Figure 12 shows the average  $Nu / Nu_0$  within zone 1 and 2 of both single spot and merging spots. In zone 1, the Nusselt number ratio increases with the dimensionless time. The average  $Nu / Nu_0$ , yielded from the single spot and merging spots increase approximately from 1.1 to 1.3 and 1.2 to 1.4, respectively within the timeframe of this research. Thus, it is about 9 % above the value obtained from a single spot at  $\tau = 120$  while 12 % are found at  $\tau = 205$ . The difference of this heat transfer capability is found to gain with the time. This can be interpreted that the combination process of the turbulent spots under the boundary layer transition can directly boost the heat transfer, finally reaching the level of turbulent flow. However, the average  $Nu / Nu_0$  in zone 2 from both single spot and merging spots characterize similarly and their values are close to 1.



**Figure 12.** The comparison of average  $Nu / Nu_0$  in zone 1 and 2 between single spot and merging spots.

As shown in figure 13, the average  $Nu / Nu_0$  over intersecting region or zone 3 of merging spots decrease from 1.4 to 1.3 or around 9.7 % during  $\tau = 120 - 140$ . After that, the average  $Nu / Nu_0$  seems to be in steady state at about 1.25 because the upstream spot has been trapped and united with the downstream spot. However, this average  $Nu / Nu_0$  is higher than those obtained from a single spot of 13.1 % - 30.5 % in this timeframe. The maximum occurs at  $\tau = 120$  and it decreases when the spots convect downstream.



**Figure 13.** The comparison of average  $Nu / Nu_0$  in zone 3 between single spot and merging spots.

The average spot effectiveness in non-intersecting zones or zone 1 and 2 of single spot and merging spots are compared as shown in figure 14. It is found that all effectiveness are higher than one and have an increasing tendency. As the characteristic of the Nusselt ration, the effectiveness of merging spots is also higher than the value from single spot. The difference is up to 5.5 % and 7.3 % for zone 1 and 3, respectively. This tendency also occurs in the intersecting region or zone 3 as shown in figure 15. The average  $Q_{ef}$  of merging spots is about 1.14 – 1.19 while the effectiveness from single spot is between 1.07 and 1.11. Therefore, these obtained results apparently show that the merging process can boost the increase of the heat transfer on the heating surface above the level of single turbulent spot.

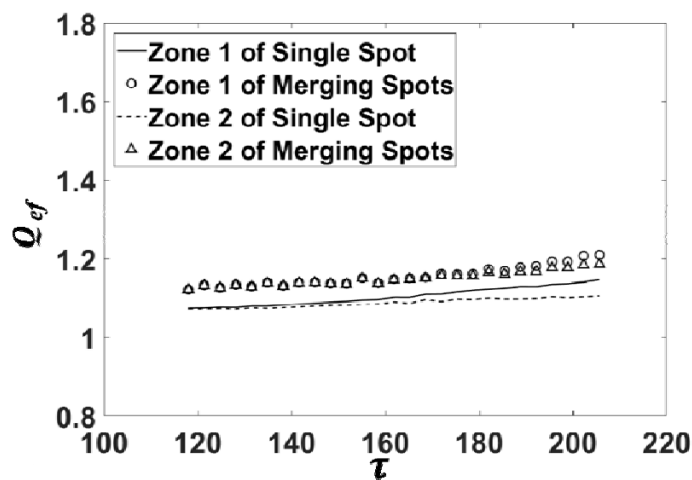


**Figure 14.** The comparison of average  $Q_{ef}$  in zone 1 and 2 between single spot and merging spots

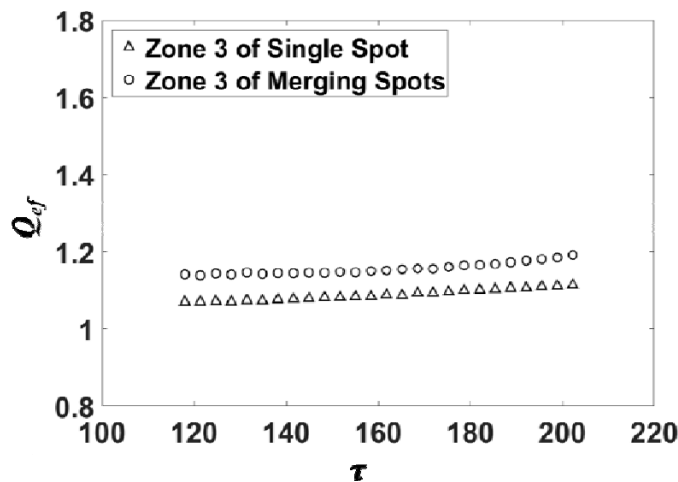


**Figure 15.** The comparison of average  $Q_{ef}$  in zone 3 between single spot and merging spots

## 5. Conclusion

Using thermochromic liquid crystals, this study presents the behavior of heat transfer enhancement via the inline merging turbulent spots induced by the small pulsating jet in perpendicular direction of the mainstream. The experiment was carried out over the isothermal surface of 28 °C during the local Reynolds number between 61,000 and 130,000 when the temperature of the mainstream is 24 °C. The results show that the  $Nu / Nu_0$  and  $Q_{ef}$  of tandem merging spots are more than those yielded from single spot. Moreover, the  $Nu / Nu_0$  over the non-intersecting zone of leading and following spots as well as the intersecting zone reveal that the heat transfer capability increases by the merging process on the region of the leading turbulent spot. Meanwhile, those over the non-intersecting zone of following spot are similar with the level of single spot. However, the increasing tendency of  $Q_{ef}$  can be observed over entire region of the merging turbulent spots. Therefore, these apparently show that the merging mechanism of the spot can directly gain the heat transfer of the heating surface above the level of single turbulent spot.

## Acknowledgement

The authors would like to acknowledge the financial support from the Thailand Research Fund (TRF) - MRG5980056 and gratefully thank Prof. Dr. Tanongkiat Kiatsirirote and Assoc. Prof. Dr. Chawalit Kittichaikarn for the valuable advices.

## References

- [1] Sabatino D and Smith C R 2008 *Journal of Fluid Mechanics* vol 612 pp 81-105
- [2] Emmons H W 1951 *Journal of Aerospace Science* vol 18 pp 490-498
- [3] Elder J W 196 *Journal of Fluid Mechanics* vol 9(2) pp 235-246
- [4] Sokolov M, Antonia R A and Chambers A J 1986 *Journal of Fluid Mechanics* vol 166 pp 211-225
- [5] Schubauer G B and Klebanoff P S 1955 *National Advisory Committee for Aeronautics Technical Note* 3489 pp 853-863
- [6] Wignanski I, Sokolov M and Friedman D 1976 *Journal of Fluid Mechanics* vol 78 pp 785-819
- [7] Wu X and Moin P 2010 *Phys. Fluids* vol 22 085105.
- [8] Makita H and Nishizawa A 2001 *Journal of turbulence* vol 2 pp 1468-5248
- [9] Krishnan L and Sandham N D 2006 *International Journal of Heat and Fluid Flow* vol 27 pp 542-550

- [10] Casper K M, Beresh S J and Schneider S P 2012 *American Institute of Aeronautics and Astronautics* pp 1-15
- [11] Reinitzer F 1888 *Wiener Monatschr Fur Chem* vol 9 pp 421-441
- [12] Abdullah N, Talib A R, Abu, Jaafar A A, Mohd Salleh M A and Chong W T 2010 *Experimental Thermal and Fluid Science* vol 34 pp 1089-1121
- [13] Wiberg R and Lior N 2004 *American Institute of Physics* vol 75(9) pp 2958-2994
- [14] Chaiworapuek W and Kittichaikarn C 2016 *International Journal of Heat and Mass Transfer* vol 92 pp 850–858
- [15] Russ J C 2002 *The image processing handbook 4<sup>th</sup> edition* (Boca Raton: CRC)
- [16] Kays W M, Crawford M E, and Weigand B 2005 *Convective Heat and Mass Transfer 4<sup>th</sup> edition* (New York: McGraw-Hill)
- [17] Rakpakdee W and Chaiworapuek W 2016 *The 7th TSME International Conference on Mechanical Engineering* (Chiang mai: Thailand)